www.amlett.com, www.vbripress.com/aml, DOI: 10.5185/amlett.2015.5801 Published online by the VBRI Press in 2015

Erbium induced raman studies and dielectric properties of Er-doped ZnO nanoparticles

C. Jayachandraiah[1*], G. Krishnaiah[2]

[1]*Department of Physics, JNTUA College of Engineering, Anantapuramu 515 002, India*
[2]*Govt. Degree College, Puttur, Chittoor 517 583, India*

[*]Corresponding author. Tel: (+91) 9642090277; E-mail: cjc_crc_ctr@yahoo.com

Received: 10 January 2015, Revised: 20 April 2015 and Accepted: 24 April 2015

ABSTRACT

Pure and erbium (1.30, 1.79, 2.83 and 3.53 at. %) doped ZnO nanoparticles are synthesized by wet chemical co-precipitation method. The synthesized samples are characterized by powder X-ray diffraction (XRD), energy-dispersive analysis of X-rays (EDAX), transmission electron microscopy (TEM), Raman spectroscopy, UV–visible diffusion reflectance spectroscopy (DRS) and LCR Impedance spectroscopy. The XRD measurements confirmed the hexagonal wurtzite structure of all samples and size of the particle is found to be decreased with Er content. TEM images show spherical shape with more agglomeration in Er doped ZnO nanoparticles. Raman spectra confirmed the hexagonal wurtzite structure of pure and Er doped ZnO nanoparticles with E_2 (high) mode at 438 cm^{-1} and presence of other possible defects. UV visible DRS shows decrease in the band gap with increasing Er^{3+} in ZnO host. Dielectric constant, dielectric loss factor and ac conductivity properties were decreased with Er dopant in tune with Maxwell -Wagner principle and surface-orientation polarizations. Copyright © 2015 VBRI Press.

Keywords: Zinc oxide; erbium; dielectric constant; nanoparticles.

Introduction

Nanometre-scale materials and semiconductors in particular seem to be important and promising in the development of next-generation electronic and optoelectronic devices [**1-3**]. The optical property of oxide semiconducting nanoparticles merely depends on the synthesis procedure and type host (ZnO, SnO_2) [**4, 5**]. Among these ZnO receives much interest due to its wide direct band gap (3.4 eV) and high excitation binding energy (60 meV) [**6**]. It is known as a multifunctional semiconductor as it can be utilized as photo catalytic, optoelectronic, piezoelectric, gas sensing and luminescence devices etc. [**7-11**]. The optical, electrical and magnetic properties of ZnO nanoparticles can be easily tuned by doping the transition elements (TM) [**12, 13**] and rare earth (RE) elements [**14, 15**]. Out of these dopants, the RE (Eu, Er, Tm, and Tb) doped semiconducting materials [**16-18**] have been intensively pursued because of 4f orbital of RE ions are shielded by the outer 6s, 5p and 5d orbitals, which weakens its coupling with the surrounding ligands [**19,20**] for the important optoelectronic device applications. For examples Tb^{3+} induces efficient visible emissions in the ZnO host [**21**].

Similarly, erbium (Er) doped ZnO nanosystems many application optical communication technology, signal amplification in waveguide, laser diodes, applications such as laser diodes and light emitting diodes (LEDs) and these applications are possible mostly due to the unique luminescence properties of Er. On other hand, electrical properties like dielectric and ac conductivity are most important properties of semiconducting material like ZnO for the application of microelectronic devices. Recently nanosystems of doped ZnO have been paid much interest in studying frequency dependent electrical properties for the applications of optoelectronic devices due to its high excitonic energy. But the reports on RE doped ZnO nanosystems are scanty. Hence, it stimulates us to synthesize Er doped ZnO nanoparticles (NPs) using low cost wet chemical co-precipitation method and study to the dielectric, ac conductivity of prepared samples for the application ZnO microelectronic devices.

Experimental

Material synthesis

Undoped and Er doped ZnO nanoparticles were prepared by a facile co-precipitation method. A high purity (99.9 %) analytical reagent (AR) grade chemicals; Zinc acetate (Zn $(CH_3COO)_2$. $2H_2O$) and erbium chloride hexahydrate (Cl_3 Er $6H_2O$) were the starting materials obtained from Sigma-Aldrich Company. Here, the dopant, erbium concentration was varied at 1.30, 1.79, 2.83 and 3.53 at % in the host matrix. Appropriate amount of precursors were dissolved in ethanol-deionized water (50-50%) with polyvinylpyrrolidone (PVP) as a surfactant and stirred for 30 min until clear solution is formed. Then, the NaOH is added to have optimum nucleation at p^H 9. This solution was transformed to hot bath of temperature 90 ^oC and stirred rigorously for 4 hours to get fine precipitation. As formed precipitation was washed 4 times with de-ionized

water and centrifuged. The precipitation was collected and dried at 80 ^{o}C for 4 hours.

Characterizations

The as-prepared samples were investigated systematically using the following analytical techniques. The composition of the prepared samples was analyzed through energy dispersive analysis of X-rays (EDAX) using Oxford Inca Penta FeTX3 EDS instrument. The structure of the powders was investigated by X-ray diffraction (XRD) measurements (D8 Advance, Bruker, Germany). The morphology was inspected by transmission electron microscope (TEM) of JEM-100CX. The crystalline nature and other related vibrational modes were carried out by Labran HR-800 Micro Raman spectrometer coupled with confocal microscope. Diffuse reflectance spectra (DRS) measurement was collected using Cary-5E UV-VIS-NIR lambda-950 spectrophotometer. For electrical measurements, a part of prepared powder has been pressed into pellets of uniform diameter and thickness. The pellets were coated by silver paste on opposite faces in order to make parallel plate capacitor geometry and sintered for 1 hour at 200^{O}C. Dielectric and impedance spectroscopy measurements were carried out by using LCR, HI-Tester (HIOKI 3532-50) at room temperature.

Results and discussion

XRD patterns of as prepared undoped and Er doped ZnO nanoparticles (NPs) are shown in **Fig. 1.** All the diffraction peaks could be well indexed to the hexagonal wurtzite structure of ZnO with JCPDS card no. 36-1451. No characteristic peaks of other impurities like Er_2O_3 are observed. The particle size of pure and Er doped ZnO nanoparticles were calculated using Scherrer formula [**22**]. The calculated particle sizes are 24, 21, 20, 18 and 17 nm respectively for pure and Er (1.30, 1.79, 2.83 and 3.53 at. %) doped ZnO nanoparticles.

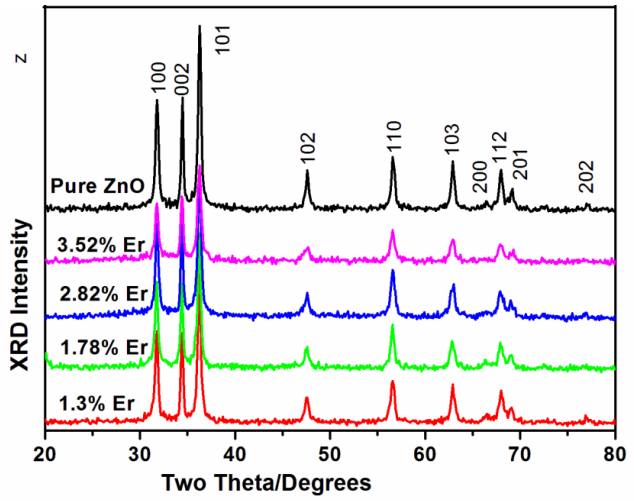

Fig. 1. XRD patterns of undoped and Er doped ZnO nanoparticles.

The morphology of undoped and 2.83 at % of Er doped ZnO nanoparticles were characterized by TEM and shown in **Fig. 2 (a** and **b)**. From the **Fig. 2**, it can be seen that the pure and Er-doped ZnO nanoparticles are similar and having nearly spherical morphology. The average diameter pure and Er doped ZnO nanoparticles are in the range of 25-20 nm which are in good agreement with calculated XRD values. The TEM image of Er doped ZnO nanoparticles show more agglomeration than pure ZnO nanoparticles.

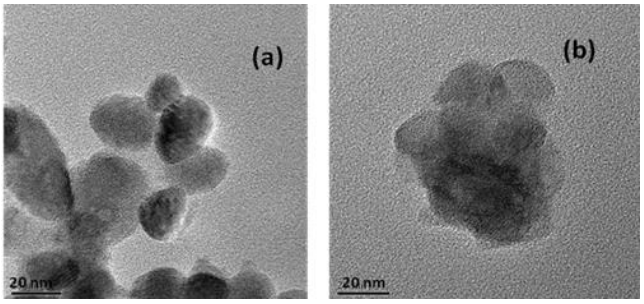

Fig. 2. Typical TEM images of (a) pure ZnO and (b) 2.83 at.% Er doped ZnO nanoparticles.

The chemical composition of the 1.79, 3.53 at % of Er doped ZnO nanoparticles were identified by EDAX and respective elemental concentrations are shown in **Fig. 3 (a** & **b)**. It revealed that the product is composed of only Zn, O and Er elements without any other contamination. It is substantiated that the height of Er peak increased with Er concentrations. Hence it is confirmed that Er ions are substituted in the host of all Er doped ZnO sample. The Er doped ZnO nanoparticles results were presented as obtained Er content from EDAX spectra.

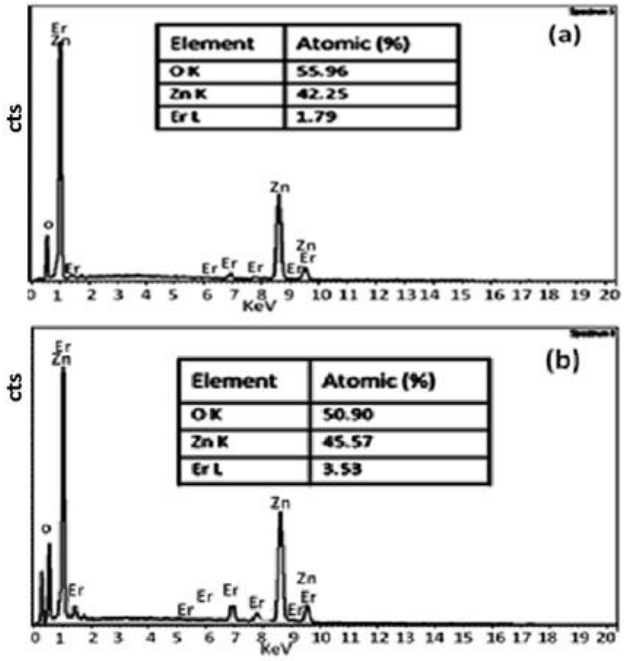

Fig. 3. EDAX spectra of (a) 1.30 at % and (b) 3.53 at % of Er doped ZnO nanoparticles.

In the wurtzite-type ZnO, the number of atoms per unit cell is s = 4, so there are a total of 12 phonon modes i.e., one longitudinal-acoustic (LA), two transverse-acoustic (TA), three longitudinal-optical (LO) and six transverse-optical (TO) branches. Since the wurtzite-type ZnO belongs to the space group c^{4}_{6v} ($P6_{3mc}$) with two formula units per

primitive cell, the optical phonons symmetries at the Γ point of the Brillouin Zone are described by the following irreducible representation **[23]**.

$\Gamma_{opt} = 1A_1 + 2B_1 + 1E_1 + 2E_2$

Where both A_1 and E_1 are Raman and infrared active modes, the E_2 modes are non-polar and Raman active and B_1 are infrared and Raman inactive modes. Both A_1 and E_1 symmetries are polar and each splits into LO and TO components with different frequencies due to the macroscopic electronic fields associated with the LO phonons. The frequency of E_2 (low) mode is associated with the vibration of the heavy Zn sub lattice, while the frequency of E_2 (high) mode involves only the oxygen atoms. In order to investigate the effect of Er on host ZnO vibrational properties are performed on all prepared undoped and Er (1.30, 1.79, 2.83 and 3.53 at. %) doped ZnO samples and results are summarized **Fig. 4**.

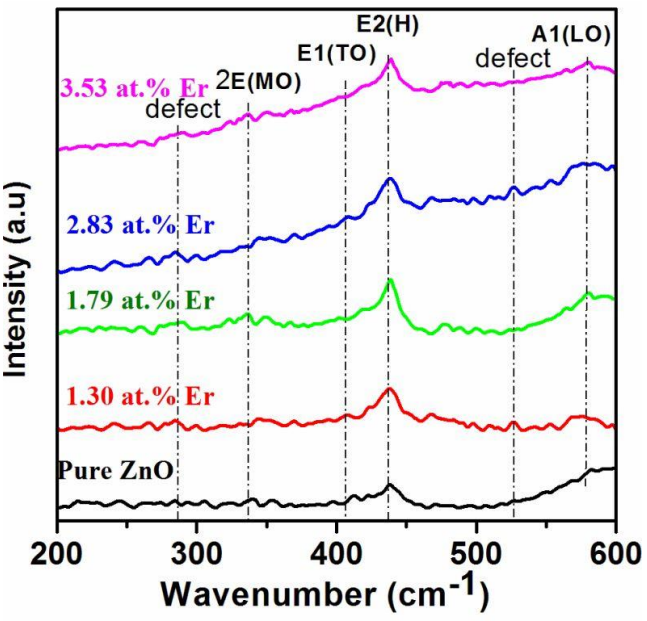

Fig. 4. Raman spectra of pure and Er doped ZnO nanoparticles.

The Raman spectra of all samples are almost similar and the observed peaks can be assigned to the optical phonon modes of ZnO wurtzite crystal structure. The band at around 438 cm^{-1} is attributed to the E_2 (high) mode of ZnO single crystalline hexagonal wurzite structure of all the samples **[23, 24]**, without significant shift. The small peak at 336 cm^{-1} is assigned to A_1 symmetry modes multiple-phonon scattering processes or [E_2 (high) - E_2 (low)]. The peaks at 579- 585 cm^{-1} are assigned to the A_1 (LO) mode and is related to host defects such as V_O and Zn_i **[23, 25]**. The peak at 381 cm^{-1} corresponds to A_1 (TO) and 406-410 cm^{-1} corresponds to E_1 (TO) modes. The anomalous vibrational modes around 520-530 cm^{-1} are appeared in Er-doped ZnO due to presence of defect concentration in the host **[24, 26]** and probably may raise from deep level emission (DLE) intensity. The minor vibrational modes around 288 cm^{-1} in Er-doped ZnO may correlate with Zn_i or V_O, induced by the impurity doping. No Raman peaks of Er_2O_3 appeared in the spectrum of the Er-doped ZnO nanostructures, indicating the absence of secondary phase as evidenced by XRD results. As it was discussed earlier, the XRD analysis of the prepared nanoparticles confirmed that all the samples possess hexagonal wurtzite structure. Therefore, as it is expected and confirmed by Raman scattering measurements, that all the samples present similar phonon responses.

The UV–Vis reflectance spectra of undoped and Er doped ZnO nanoparticles are presented in **Fig. 5 (a)**. The undoped ZnO has high reflectance in the range between 450 to 700 nm, while the Er doped ZnO nanoparticles had several bands at 450 nm 487 nm, 521 nm, 530 nm and 650 nm indicates the transition among excited levels ($^2F_{3/2}$), ($^4F_{5/2}$), ($^4F_{7/2}$), $^4H_{11/2}$), ($^4F_{9/2}$) and ground level ($^4I_{15/2}$) of substituted Er dopant ions **[27]**. It is noticed from the spectra that the UV absorption end was shifted towards the lower energy side with increase in Er concentration. Furthermore, the energy band gap of ZnO: Er nanoparticles could be estimated using Kubelka-Munk function $[F(R)h\upsilon]^2$ **[28]** and is shown in **Fig. 5 (b)**. To calculate the direct band gap energy (hυ in eV), the linear part of the curve was extrapolated to F(R) =0 where F(R) = $[(1-R)^2/2R]$, R is reflectance value for corresponding wavelength. The estimated E_g values of pure and Er doped ZnO nanoparticles are 3.30, 3.291, 3.274, 3.272 and 3.270 eV respectively. It is found that the band gap values of the Er doped ZnO nanoparticles are lower than that of pure ZnO (3.30eV).

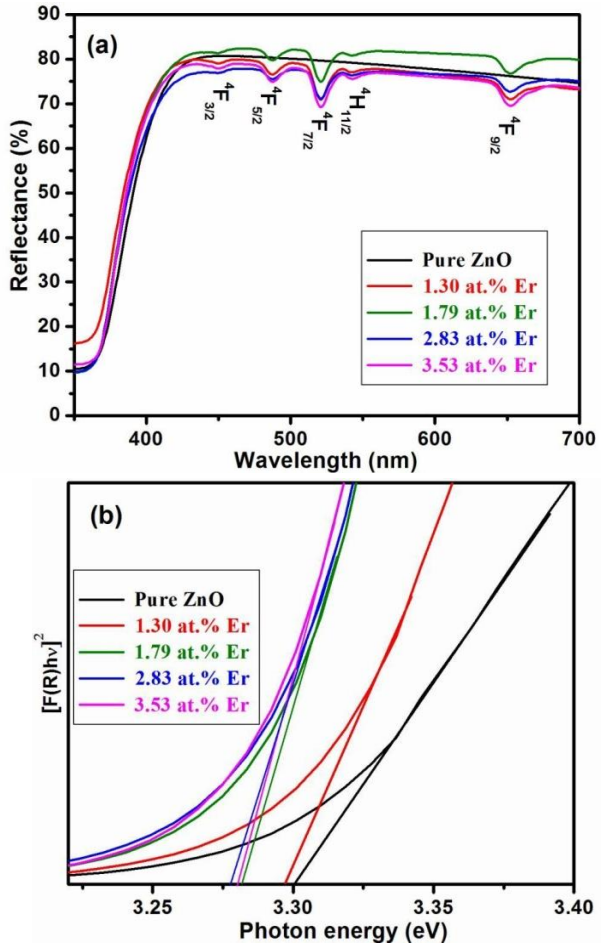

Fig. 5. UV-Visible DRS of (a) reflectance spectra and (b) Energy band gap profiles of pure and Er doped ZnO nanoparticles.

The decrease in the band gap is not due to quantum confinement effect **[5]** and it is due to appearance of new electronic states among ZnO band gap value due to the addition of rare earth activator (Er) ion. When of rare earth activator Er ion incorporated into ZnO matrix, the Er electron localized states are formed and introduce new states closer to conduction band which in turn reduces the band gap of ZnO **[29]**.

The dielectric constant is an important property of a material that affects many optoelectronic and transport properties. Frequency variation dielectric constant (ε_r) plots of pure and Er doped ZnO NPs is shown in the **Fig. 5**. Different frequency responses of dielectric constants are calculated by using the fallowing formula **[30]**;

$$\varepsilon_r = \frac{C_p d}{\varepsilon_0 A}$$

where, C_p is the capacitance, d is thickness and A is area of the prepared pellet samples. ε_o is the permittivity of free space and its value is 8.85×10^{-12} F/m.

As shown in **Fig. 6**, the observed dielectric constant is high at low frequency region and decreased with increase in frequency. This type of behavior can be explained by Maxwell-Wagner model **[31]** for homogeneous double structure. According to this model, the dielectric medium is composed of well conducting grains and separated by poor conducting walls. Under external electric field the charge carriers can travel freely in the grain and accumulate at the grain boundary. The accumulations of charge carriers are high at lower frequency of applied field with small conduction of charge carriers at the grain boundaries. But the charge carriers do not fallow the applied field phase at higher frequency which results in decrease of dielectric constant. This may also explained on surface charge polarization due to structural inhomogeneities of nanoparticles at lower frequency, while the higher frequency region ε_r is explained based on ionic (rotation of dipoles) polarization **[32, 33]**.

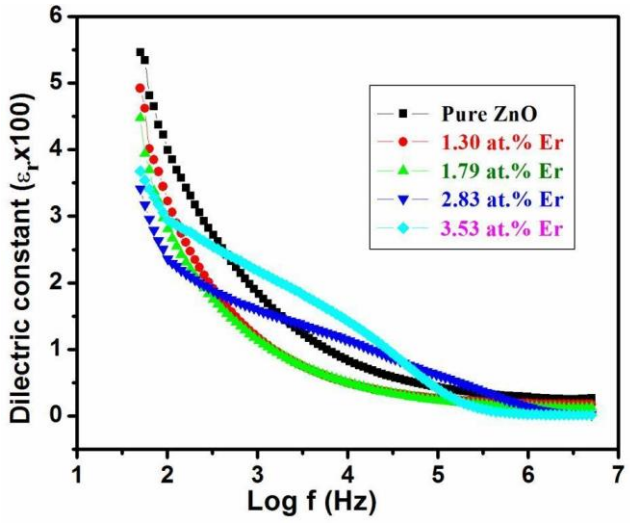

Fig. 6. Frequency variation dielectric constant of Er doped ZnO nanoparticles.

It is noticed that the dielectric constant is decreased in Er doped ZnO in compared with pure ZnO. The dielectric constant decreased in the whole applied frequency region with Er dopant up to 1.79 at %. Because, the polarization is decreased due to the formation of grains surrounded by insulating grain boundaries, while ε_r is slightly increased in the medium frequency range for 2.83 and 3.53 at.% of Er dopant. It indicates that the dominant ionic polarization over the space charge polarization **[34]** in the applied frequency range 1kHz - 1000 kHz for higher Er dopant concentration. The possible source of orientation polarization is the existence oxygen vacancies and zinc interstitials in the nano-sized ZnO. The oxygen vacancies are increased in the crystal field with increasing diffusion of Er content, which leads to an increase of dipole moment and in turn the orientation of polarization.

Fig. 7 shows the variation of corresponding imaginary dielectric constant (ε') values of pure and Er doped ZnO NPs as a function of frequency. It can be calculated by the following relation [**30**].

$$\varepsilon' = \varepsilon_r \tan\delta$$

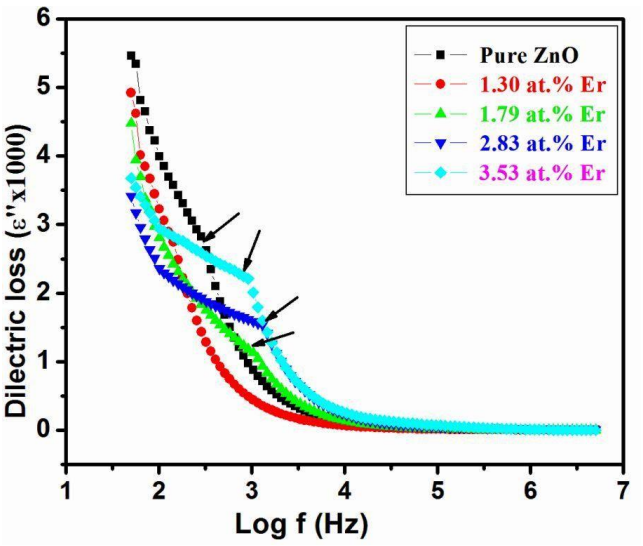

Fig. 7. Frequency variation dielectric loss of Er doped ZnO nanoparticles.

Where, tanδ is dielectric loss and it is proportional to imaginary dielectric constant. It can be seen that, ε' values decrease with the increase of frequency for pure and Er doped ZnO NPs which might be due to the space charge polarization. It is also clear from the **Fig. 7** that the losses are decreased with Er doping in the ZnO NPs. Hence, it can be concluded that the Er doped ZnO NPs are very important for high frequency applications.

All NPs display one peak (indicated with arrows in the **Fig. 7**) at certain frequency which is shifted to higher frequency with lower Er doping (up to 1.79 at %) and shifted to lower frequency for higher doping (beyond 1.79 at %). This peaking behavior explains the relaxation process of the hopping of localized charge carriers. The angular frequency (ω) is inversely proportional to relaxation time (τ) and directly proportional hopping probability (p) of charge carriers at grain boundaries [**34**]. Therefore increase in frequency of relaxation peak denotes decrease in dielectric constant as shown in **Fig. 6.**

The frequency dependent ac conductivity (σ_{ac}) variation of different pellets of Er doped ZnO NPs are shown in the

Fig. 8 and it can be calculated using the following relation **[30]**.

$\sigma_{ac} = \omega\varepsilon_0\varepsilon_r \tan\delta$

where, ω is the angular frequency of the applied field. It has been observed clearly from the plots that the ac conductivity increases as the frequency of applied ac field increases for all pure and Er doped ZnO NPs, because the increase in frequency of ac applied field enhances the hopping of charge carriers.

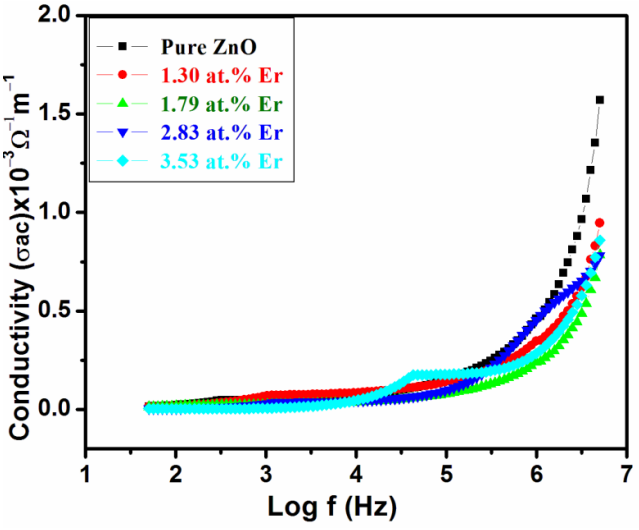

Fig. 8. Frequency variation ac conductivity of Er doped ZnO nanoparticles.

It is also evident from **Fig. 8** that ac conductivity is initially high for pure ZnO and found to be less in Er doped ZnO NPs. The substitution of Er dopant may initiate the defect ions, oxygen vacancies in the ZnO NPs and tends to segregate at the grain boundaries due to the diffusion at the time of sintering and cooling processes. These defects block the flow of charge carriers at the grain boundaries and cause decrease in the conductivity initially up 1.79 at % of Er doping the materials **[30]**. Thereafter the conductivity increases. It is due to the fact that the increase in dopant concentration increases the rate of hopping process of charges of Er^{3+} which predominated over charge carriers blocking effect **[22, 35]**.

Conclusion

The pristine and Er doped ZnO nanoparticles are successfully synthesized by chemical co-precipitation method. All samples are crystallized in the hexagonal wurtzite structure of ZnO without any impurity phases. The presences of Er in the ZnO nanoparticles are confirmed by EDAX. The XRD measurements confirmed the hexagonal wurtzite structure of all samples with decreasing particle size from 23 nm to 17 nm with increasing Er dopant concentration. TEM images are exhibiting spherical shape of nanoparticles with average particle size 20-25 nm and are in good agreement with XRD values. The Raman spectra show hexagonal wurtzite structure of all prepared samples. DRS spectra revealed that the energy gap is decreased with increasing Er doping due the formation of new electronic states of Er^{3+} ions in the band gap. Dielectric constant and ac conductivity are decreased with Er doping and showing an interesting dielectric properties and ac conductivity at medium applied frequency range as well as higher Er dopant content. Hence, these properties are significant for the application of microelectronic devices.

Acknowledgements

One of the authors Dr. G. Krishnaiah is thankful to UGC (SERO), Hyderabad, India for providing financial support [Link No.4381] to carry out present research work. The authors also express thanks to CSIR-Central Electrochemical Research Institute (CECRI), Karaikudi – 630006, Tamil Nadu, India for providing the electrical measurements.

Reference

1. M. Nirmal, L.E. Brus, *Acc. Chem. Res.* **1999**, *32*, 407. **DOI:** 10.1021/ar9700320
2. A.P. Alivisatos, *Science*, **1996**, *271*, 933. **DOI:** 10.1126/*science*.271.5251.933.
3. S. Kumar, P.D. Sahare, *J. Rare Earths*, **2012**, *30*, 761. **DOI:** 10.1016/S1002-0721(12)60126-4
4. Kumar, V.; Swart, H.C.; Gohain, M.; Som, S.; Bezuindenhoudt, B.C.B.; Ntwaeaborwa, O.M.; *Ultrason. Sonochem.*, **2014**, *21*, 1549. **DOI:** 10.1016/j.ultsonch.2014.01.019
5. Kumar, V.; Kumar, V.; Som, S.; Neethling, J.H.; Lee, M.; Ntwaeaborwa, O.M.; Swart; H.C.; *Nanotechnol.*, **2014**, *25*, 135701. **DOI:** 10.1088/0957-4484/25/13/135701
6. Park, Y.S.; Litton, C.W.; Collins, T.C.; Reynolds, D.C.; *Phys. Rev.*, **1966**, *143*, 512. **DOI:** 10.1103/PhysRev.143.512
7. Moon, T.H.; Jeong, M.C.; Lee, W.;. Myoung. J.M; *Appl. Surf. Sci.* **2005**, *240*, 280. **DOI:** 10.1016/S0169-4332(05)00957-8
8. Hong, R.Y.; Li, J.H. ; Chen, L.L.; Liu, D.Q.; Li, H.Z., Zheng, Y.; Din, J.; *Powder Technol*., **2009,** *189*, 426. **DOI:** 10.1016/*j*.powtec.2008.07.004
9. Kuriakose, S; Satpati, B; Mohapatra, S; *Adv. Mater. Lett*. **2015**, *6(3)*, 217. **DOI:** 10.5185/amlett.2015.5693
10. Jin, B.J.; Bae, S.H.; Lee, S.Y.; Im, S.; *Mater. Sci. Eng., B,* **2000,** *71*, 305. **DOI:** 10.1016/S0921-5107(99)00395-5
11. Irimpan, L.; Nampoori, V.P.N.; Radhakrishnan, P.; Deepthy, A.; Krishnan, B.; *J. Appl. Phys.*, **2007,** *102*, 063524. **DOI:** 10.1063/1.2778637
12. Kaur, G.; Mitra, A.; Yadav. K.L.; *Adv. Mater. Lett*., **2015,** *6(1)*, 73**.** **DOI:** 10.5185/amlett.2015.5606
13. Reddy, B.S.; Reddy, S.V.; Reddy, N.K.; Reddy, Y.P.; *Adv. Mater. Lett.* **2014, *5(4)*, 199.** **DOI:** 10.5185/amlett.2013.8529
14. Ajimsha, R.S.; Das, A.K.; Singh, B.N.; Misra, P.; Kukreja, L.M.; *Phys. E*, **2010,** *42*, 1838. **DOI:** 10.1016/j.physe.2010.02.005
15. Ohtake, T.; Hijii, S.; Sonoyama, N.; Sakata. T.; *Appl. Surf. Scie.*, **2006,** *253*, 1753. **DOI:** 10.1016/j.apsusc.2006.03.008
16. Subramanian, M.; Thakur, P.; Gautam, S.; Chae, K.H.; Tanemura, M.; Hihara, T.; Vijayalakshmi, S.; Soga, T.; Kim, S.S.; Asokan, K.; Jayavel, R.; *J. Phys. D: Appl. Phys.* **2009,** *42*, 105410. **DOI:** 10.1088/0022-3727/42/10/105410
17. Chen, W.; Zhang, J.; *J. Nanosci. Nanotech.* **2006,** *6*, 1159. **DOI:** 10.1166/jnn.2006.327
18. Som, S.; Kunti, A.K.; Kumar, V.; Kumar, V.; Dutta, S.; Chowdhury, M.; Sharma, S.K.; Terblans, J.J.; Swart, H.C.; *J. Appl.* **2014,** *115*, 193101. **DOI:** 10.1063/1.4876316
19. Kumar, N.; Kumar, V.; Swart, H.C.; Mishra, A.K.; Ngila, J.C.; Parashar; V.; *Mater. Lett.* **2015,** *146*, 51. **DOI:** 10.1016/j.matlet.2015.01.150
20. Mordkovich, V.Z.; Hayashi, H.; Haemori, M.; Fukumura, T.; Kawasaki, M.; *Adv. Funct Mater.* **2003,** *13*, 519. **DOI:** 10.1002/adfm.200304335

21. Kumar, V.; Som, S.; Kumar, V.; Kumar, V.; Ntwaeaborwa, O.M.; Coetsee, E.; Swart, H.C.; *Chem. Eng. J.*, **2014**, *255*, 541. **DOI:** 10.1016/j.cej.2014.06.027
22. R.D. Shannon, *J. Appl. Phys.*, **1993,** *73*, 348. **DOI:** 10.1063/1.353856
23. Umar, A.; Suh, E.K.; Hahn, Y.B.; *Solid State Commun.* **2006,** *139*, 447. **DOI:** 10.1016/j.ssc.2006.07.014
24. Lin, X.X.; Zhu, Y.F.; Shen, W.Z.; *J. Phys. Chem. C*, **2009,** *113* 1812. **DOI:** 10.1021/jp810134h
25. Tseng, Y.C. ; Lin, Y.J.; Chang, H.C.; Chen, Y.H.; Liu, C.J.; Zou, Y.Y.; *J. Lumin.*, **2012,** *132*, 1896. **DOI**: 10.1016/j.jlumin.2012.03.009
26. P. Kumar, J. P. Singh, Y. Kumar, A. Gaur, H.K. Malik, K. Asokan, *Curr. Appl. Phys.*, **2012,** *12*, 1166. **DOI**: 10.1016/j.cap.2012.02.042
27. Ji, S.; Yin, L.; Liu, G.; Zhang, L.; Ye, C.; *J. Phys. Chem*. C, **2009,** *113*, 16439. **DOI: 10.**1021/jp906501n
28. Chen, Y.; Xu, X.L.; Zhang, G.H.; Xue, H.; Ma, S.Y.; *Physica E.*, **2010**, *42*, 1713. **DOI:** 10.1016/j.physe.2010.01.029
29. Anandan, S.; Miyauchi, M.; *Phys. Chem. Chem. Phys.*, **2011**, *13*, 14937. **DOI:** 10.1039/c1cp21514k
30. Ansari, S.A.; Nisar, A.; Fatma, B.; Khan, W.; Naqvi, A.H.; *Mater. Sci. Eng. B* **2012,** *177*, 428. **DOI:** 10.1016/j.mseb.2012.01.022
31. Prodromakis, T.; Papavassiliou, C.; *Appl. Surf. Sci.*, **2009,** *255*, 6989. **DOI**: 10.1016/j.apsusc.2009.03.030
32. Lanje, A.S.; Sharma, S.J.; Ningthoujam, R.S.; Ahn, J.S.; Pode, R.B.; *Adv. Powder Technol*, **2013,** *24*, 331. **DOI**: 10.1016/j.apt.2012.08.005
33. Zamiria, R.; Singh, B.K.; Dutta, D.; Reblo, A.; Ferreira, J.M.F.; *Ceram. Int.*, **2014,** *40*, 4471. **DOI:** 10.1016/j.ceramint.2013.08.120
34. Watawe, S.; Sarwade, B.; Bellad, S.; Sutar, B.; Chougule, B.; *J. Magn. Magn. Mater.* **2000,** *214 (1)*, 55. **DOI**: 10.1016/S0304-8853(00)00033-0
35. Azam, A.; Ahmed, A.S.; Ansari, M.S.; Shafeeq, M.; Naqvi, A.H.; *J. Alloys Compounds*, **2010,** *506*, 237. **DOI:** 10.1016/j.jallcom.2010.06.184